Ocean Engineering

Ocean Engineering

Trajectory tracking control of ROVs considering external disturbances and measurement noises using ESKF-based MPC

Chengqi Long [a], Xiaohui Qin [a] , Yougang Bian[a] , Manjiang Hu [a*]

[a]*State Key Laboratory of Advanced Design and Manufacturing for Vehicle Body, College of Mechanical and Vehicle Engineering, Hunan University, Changsha, 410082, China.*

**Corresponding author: College of Mechanical and Vehicle Engineering, Hunan University, Changsha, 410082, China.*

Abstract

This paper proposes a tracking method aiming at trajectory tracking for a remotely operated underwater vehicle (ROV) under external disturbances and measurement noises. Firstly, the six-degree-of-freedom kinematics model and dynamics model of the ROV are proposed to derive the discrete-time varying nonlinear model, where the Euler method is used and the assumption that the center of gravity of the ROV coincides with the center of buoyancy is made. The external disturbance representing ocean current is explicitly considered in the form of velocities instead of forces in the dynamics model to avoid the problem that forces on the ROV caused by ocean current are difficult to measure. Secondly, an extended state based Kalman filter (ESKF) is constructed to estimate system states and external disturbances in the presence of measurement noises and the filter gain is automatically tuned by the Kalman filter technique, which can greatly improve the estimation accuracy. Thirdly, the ESKF-based model predictive control (MPC) controller is newly formulated, and an objective function under linear time-invariant (LTI) constraints is constructed based on the tracking error and the desired control input increment to ensure the accuracy and prevent damage to actuators. Finally, the performance of the proposed method is verified by numerical simulations.

Keywords: Remotely operated underwater vehicle; Trajectory tracking; Model predictive control; External disturbance; Measurement noise

* E-mail addresses: whkxa_618_ybz@163.com (Chengqi Long), qxh880507@163.com (Xiaohui Qin), byg10@foxmail.com (Yougang Bian), manjiang_h@hnu.edu.cn (Manjiang Hu).

1. Introduction

Remotely operated underwater vehicles (ROVs) are widely used in the exploration of territory, mining of marine resources (Choyekh et al., 2015), the laying of submarine cables and the maintenance of underwater artificial facilities (Tsukioka et al., 2015), without the need for real time human operations, which can significantly improve operational safety and efficiency (Fossen et al., 2006). The ROV performs tasks usually based on the control instructions sent by the operator on the sea mother ship through cables. However, the performance of the ROV without automatic control function is relatively poor when completing difficult tasks such as three-dimensional trajectory tracking (Soylu et al., 2016), which is a typical underwater operation in pipeline inspection and mineral handling (Zhou et al., 2017).

Currently, many methods have been proposed in trajectory tracking, such as proportional-integral-derivative (PID) control, backstepping control (BSC), fuzzy logic control (FLC), adaptive control, sliding mode control (SMC), neural network control (NNC) (Boehm et al., 2020; Chu et al., 2016). Due to the ease of practical implementation, PID control has been widely used in underwater vehicle control. Kim et al. (2013) proposed a dual-loop variable-structure controller with anti-windup, it fed the difference between the target input and force limits back to the integral term, which could reduce the integral-windup effect. Khodayari and Balochian (2015) introduced a new self-adaptive fuzzy PID controller based on nonlinear structure with multiple input and multiple output (MIMO), which combined an adaptive method and a dual PID controller, improving the performance with parametric uncertainties and model uncertainties. However, PID control cannot provide accurate trajectory tracking even if it tracks a linear second-order desired trajectory. At the same time, PID cannot cope with nonlinear models and uncertain external disturbances. SMC can make the system states reach and slide along the sliding mode surface in a finite time by switching control variables, without being affected by parameter perturbations and external disturbances. Wang et al. (2011) proposed a nonlinear iterative sliding mode controller and established the equation of horizontal tracking error for an under-actuated autonomous underwater vehicle (AUV) to overcome singular value. Simulation results proved that the path tracking method was effective and the under-actuated AUV could track the desired horizontal path precisely. Qiao and Zhang (2019) designed two adaptive integral terminal sliding mode control frameworks to control an unmanned underwater vehicle (UUV) to track desired trajectories. This control framework could improve tracking accuracy and enhance robustness to parametric uncertainties and external disturbances. However, SMC may cause high-frequency oscillation called “chattering” on the sliding mode surface, resulting in low control accuracy and high energy consumption. FLC can make machines reason like humans. Dai et al. (2002) proposed a three-layer fuzzy logic controller for ROV navigation, which resulted in smooth motion control and robust performance. Liu et al. (2012) introduced a novel path planning algorithm based on fuzzy logic for AUV in 3D unknown space and simulation results demonstrated the effectiveness of the method. Sun et al. (2018) proposed a three-dimensional trajectory planning method based on an optimized fuzzy control algorithm, which could achieve good planning results in complex underwater environments. However, the design of FLC fuzzy rules relies heavily on subjective experience, which brings contingency to the control effect. BSC has good robustness to parametric uncertainties and system nonlinearities. Repoulias and Papadopoulos (2006) developed a two-dimensional planar trajectory tracking method based on backstepping technology for AUV, which kept the tracking error within a small area of zero. Zain et al. (2014) considered a nonlinear control method for stabilizing all attitudes and positions of an underactuated X4-AUV with four thrusters and six-degree-of-freedom, the controlled system could be robustly stabilized for all the time. However, the computational complexity of BSC will increase rapidly as the order of the system increases. NNC can improve the adaptive learning ability of the system and has been extensively studied. Mon and Lin (2012) developed a guidance law based on supervisory recurrent fuzzy neural network control (SRFNNC) for AUV guidance systems. Simulation results showed that the proposed SRFNNC guidance law was robust and could obtain high accuracy. Cui et al. (2017) integrated two neural networks into an adaptive

controller that took control input nonlinearities, model uncertainties and external disturbances into account, this method achieved good effectiveness and robustness. However, the control performance of NNC depends on the number of neural network nodes, resulting in a large amount of calculation, which is not suitable for practical engineering applications.

Further analysis of the methods mentioned above shows that the above methods have some common shortcomings. These methods cannot deal with constraints on system states and propulsion in the control process, which may cause poor tracking performance. In addition, these methods are also unable to solve the trajectory tracking problem considering external disturbances and measurement noises.

MPC is a closed-loop optimization control strategy that can solve control problems with extra constraints on control inputs and system states, as well as real-time external disturbances (Yan et al., 2020). It has become a powerful framework for the trajectory tracking of underwater vehicles (Bai et al., 2019). Molero et al. (2011) proposed a trajectory tracking method for a six-degree-of-freedom ROV based on MPC, which could reduce tracking error by 40% compared to PID controllers. Zhu and Xia (2016) developed an adaptive MPC for unconstrained discrete-time linear systems with parametric uncertainties. The adaptive MPC combined an adaptive updating law for estimated parameters and a constrained MPC for an estimated system. Simulation results showed that the adaptive MPC could deal with parametric uncertainties. Shen et al. (2017a) developed a novel Lyapunov-based MPC (LMPC) framework for an AUV to improve the trajectory tracking performance. Simulation results on the Saab SeaEye Falcon AUV model demonstrated that this method significantly enhanced trajectory tracking control performance. Shen et al. (2017b) designed a nonlinear MPC controller that could simultaneously solve the problem of trajectory planning and tracking, and the effectiveness of the method was proved by experiments. Zhang et al. (2019) used an MPC controller to track trajectories with the constraints of actuator saturation and system state boundaries. The ocean current disturbance is introduced in the simulation to verify the effectiveness and robustness of the control method. However, these proposed trajectory tracking methods did not consider the influence of external disturbances and measurement noises at the same time, which could not guarantee tracking accuracy.

To settle the above mentioned problem, we newly propose an ESKF-based MPC based ROV tracking method, considering ocean current disturbances and measurement noises simultaneously, which can ensure tracking accuracy and robustness in real implementations. The main contributions of this work are:

1. Ocean current disturbances are introduced into the dynamics model in the form of velocity rather than forces, which helps avoid the problem that it is difficult to measure forces on ROV applied by ocean current. In addition, it is beneficial for improving tracking accuracy during ROV operations.

2. The ESKF is constructed to estimate system states and external disturbances in the presence of measurement noises, which is good for improving the robustness of the ROV against external disturbances.

3. The discrete-time varying nonlinear model of ESKF-based MPC is derived based on the ROV kinematics model and dynamics. Measurement noises are introduced into the output equation so that they can be taken into account in the objective function established later, which can make the tracking algorithm robust to measurement noises.

4. Applying the tracking error and the control input increment to construct an objective function under LTI constraints on the propulsion increment, which can ensure tracking accuracy and avoid damage to actuators.

The rest of the paper is organized as follows: Section 2 introduces the kinematics model and dynamics model for ROV. Section 3 shows the details of the ESKF-based MPC controller. Simulation results are provided in Section 4 to validate the proposed method. Finally, Section 5 concludes the paper.

2. ROV modeling

This section introduces the kinematics model and the dynamics model for the proposed ESKF-based MPC controller. These two models are used to derive the discrete-time nonlinear time varying model of ESKF-based MPC in Section 3.

2.1. Kinematics model

The kinematics model of the ROV is constructed in order to derive the state prediction equation of MPC. As shown in Fig.1, in order to numerically describe the position, attitude and velocity of the ROV, an inertial reference frame and a body frame are defined, using the right-handed coordinate system. The inertial reference frame is fixed with O_g being its origin. The origin of the body frame is O_b and it coincides with the ROV gravity center.

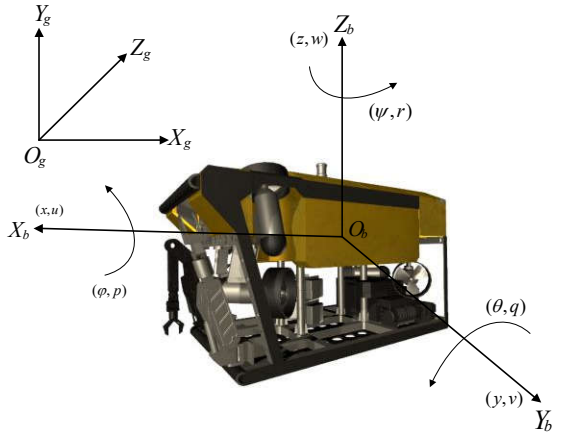

Fig.1. ROV coordinate system

The ROV studied in this paper has 4 horizontal propellers and 3 vertical propellers. As shown in Fig. 2, the axis of each horizontal propeller is parallel to the horizontal plane, and the angle between it and axis X_b is 45 degrees. The axis of each vertical propeller is parallel to the vertical plane, and the angle between it and axis Z_b is 15 degrees.

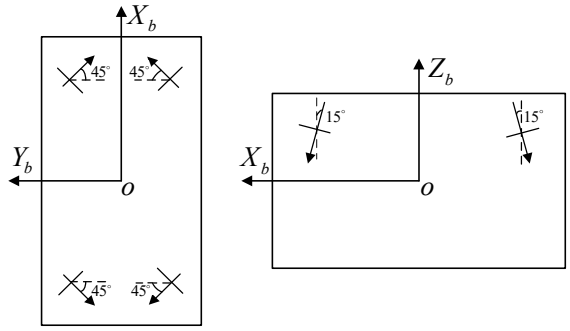

Fig. 2. Propeller layout diagram

The position and attitude of the ROV are denoted by vector $S = [x, y, z, \varphi, \theta, \psi]^{\mathrm{T}}$, where x, y, and z are translation motions along axes X_g, Y_g, and Z_g, and φ, θ , and ψ represent rotations of the ROV around axes X_g, Y_g, and Z_g, respectively. The velocity vector of the ROV is expressed as $V = [u, v, w, p, q, r]^{\mathrm{T}}$, where u, v, and w are the linear velocity along axes X_b, Y_b, and Z_b, and p, q , and r are the angular velocity around X_b, Y_b, and Z_b, respectively. The relationship between S and V can be expressed as follows:

$$\dot{S} = GV \tag{1}$$

where

$$G = \begin{bmatrix} G_1 & O_{3\times3} \\ O_{3\times3} & G_2 \end{bmatrix} \tag{2}$$

$$G_1 = \begin{bmatrix} a_{11} & a_{12} & a_{13} \\ a_{21} & a_{22} & a_{23} \\ a_{31} & a_{32} & a_{33} \end{bmatrix} \tag{3}$$

$$G_2 = \begin{bmatrix} b_{11} & b_{12} & b_{13} \\ b_{21} & b_{22} & b_{23} \\ b_{31} & b_{32} & b_{33} \end{bmatrix} \tag{4}$$

$a_{11} = \cos\theta\cos\psi$, $a_{12} = \sin\varphi\sin\theta\cos\psi - \cos\varphi\sin\psi$, $a_{13} = \cos\varphi\sin\theta\cos\psi + \sin\varphi\sin\psi$, $a_{21} = \cos\theta\sin\psi$, $a_{22} = \sin\varphi\sin\theta\sin\psi + \cos\varphi\cos\psi$, $a_{23} = \cos\varphi\sin\theta \cdot \sin\psi - \sin\varphi\cos\psi$, $a_{31} = -\sin\theta$, $a_{32} = \sin\varphi\cos\theta$, $a_{33} = \cos\varphi\cos\theta$, $b_{11} = 1$, $b_{12} = \sin\varphi\tan\theta$, $b_{13} = \cos\varphi\tan\theta$, $b_{21} = 0$, $b_{22} = \cos\varphi$, $b_{23} = -\sin\varphi$, $b_{31} = 0$, $b_{32} = \sin\varphi\sec\theta$, $b_{33} = \cos\varphi\sec\theta$.

G is the conversion matrix from the body frame to the inertial reference frame, G_1 is the linear velocity conversion matrix, and G_2 is the angular velocity conversion matrix.

2.2. Dynamics model

The dynamics model of the ROV is used to compute the relationship between the desired motion of the ROV and the forces executed by actuators. In the paper, we introduce ocean current into the dynamics model in order to improve tracking accuracy. However, compared to the forces on ROV caused by ocean current, the ocean current velocity is relatively easy to measure. Denote by d_c the ocean current disturbance on the ROV in the body frame. Then the ROV dynamics model is as follows:

$$M\dot{V} + C(V - d_c) + D(V - d_c) + R = \tau \tag{5}$$

where $M = M_{RB} + M_A$ is the inertia matrix (Shen et al., 2017), $M_{RB} = \mathrm{diag}(m, m, m, I_x, I_y, I_z)$is the rigid body mass matrix, m is the mass, I_x, I_y , and I_z are

the moments of inertia regarding to X_b, Y_b, and Z_b, respectively, $M_A = -\mathrm{diag}(X_{\dot{u}}, Y_{\dot{v}}, Z_{\dot{w}}, K_{\dot{p}}, M_{\dot{q}}, N_{\dot{r}})$ is the hydrodynamic additional mass matrix, and $X_{\dot{u}}$, $Y_{\dot{v}}$, $Z_{\dot{w}}$, $K_{\dot{p}}$, $M_{\dot{q}}$, $N_{\dot{r}}$ are hydrodynamic coefficients. The function diag is used to construct a diagonal matrix.

Here $C = C_{RB} + C_A$ is the rigid body centripetal and Coriolis matrix, where C_{RB} is the rigid body centripetal force and Coriolis force matrix, and C_A is the hydrodynamic centripetal force and Coriolis force matrix, of which the expressions are as follows:

$$C_{RB} = \begin{bmatrix} C_{RB1} & C_{RB2} \\ C_{RB3} & C_{RB4} \end{bmatrix} \tag{6}$$

$$C_A = \begin{bmatrix} C_{A1} & C_{A2} \\ C_{A3} & C_{A4} \end{bmatrix} \tag{7}$$

where

$$C_{RB1} = \begin{bmatrix} 0 & 0 & 0 \\ 0 & 0 & 0 \\ 0 & 0 & 0 \end{bmatrix} \tag{8}$$

$$C_{RB2} = \begin{bmatrix} 0 & m(w-d_{cz}) & -m(v-d_{cy}) \\ -m(w-d_{cz}) & 0 & m(u-d_{cx}) \\ m(v-d_{cy}) & -m(u-d_{cx}) & 0 \end{bmatrix} \tag{9}$$

$$C_{RB3} = \begin{bmatrix} 0 & m(w-d_{cz}) & -m(v-d_{cy}) \\ -m(w-d_{cz}) & 0 & m(u-d_{cx}) \\ m(v-d_{cy}) & -m(u-d_{cx}) & 0 \end{bmatrix} \tag{10}$$

$$C_{RB4} = \begin{bmatrix} 0 & I_z(r-d_{cr}) & -I_y(q-d_{cq}) \\ -I_z(r-d_{cr}) & 0 & I_x(p-d_{cp}) \\ I_y(q-d_{cq}) & -I_x(p-d_{cp}) & 0 \end{bmatrix} \tag{11}$$

$$C_{A1} = \begin{bmatrix} 0 & 0 & 0 \\ 0 & 0 & 0 \\ 0 & 0 & 0 \end{bmatrix} \tag{12}$$

$$C_{A2} = \begin{bmatrix} 0 & -Z_{\dot{w}}(w-d_{cz}) & Y_{\dot{v}}(v-d_{cy}) \\ Z_{\dot{w}}(w-d_{cz}) & 0 & -X_{\dot{u}}(u-d_{cx}) \\ -Y_{\dot{v}}(v-d_{cy}) & X_{\dot{u}}(u-d_{cx}) & 0 \end{bmatrix} \tag{13}$$

$$C_{A3} = \begin{bmatrix} 0 & -Z_{\dot{w}}(w-d_{cz}) & Y_{\dot{v}}(v-d_{cy}) \\ Z_{\dot{w}}(w-d_{cz}) & 0 & -X_{\dot{u}}(u-d_{cx}) \\ -Y_{\dot{v}}(v-d_{cy}) & X_{\dot{u}}(u-d_{cx}) & 0 \end{bmatrix} \tag{14}$$

$$C_{A4} = \begin{bmatrix} 0 & -N_{\dot{r}}(r-d_{cr}) & M_{\dot{q}}(q-d_{cq}) \\ N_{\dot{r}}(r-d_{cr}) & 0 & -K_{\dot{p}}(p-d_{cp}) \\ -M_{\dot{q}}(q-d_{cq}) & K_{\dot{p}}(p-d_{cp}) & 0 \end{bmatrix} \tag{15}$$

where d_{cx} , d_{cy} , d_{cz} , d_{cp} , d_{cq} , and d_{cr} are the translation and rotation components of d_c along the three coordinate axes. Here d_c is converted from ocean current disturbance d_{cg} in the inertial reference frame, and is described as follows:

$$d_c = G^{-1} d_{cg} \tag{16}$$

where G^{-1} is the inverse of G.

$D = \mathrm{diag}(X_u + X_{|u|u}|u - d_{cx}|, Y_v + Y_{|v|v}|v - d_{cy}|, Z_w + Z_{|w|w}|w - d_{cz}|, K_p + K_{|p|p}|p - d_{cp}|, M_q + M_{|q|q}|q - d_{cq}|, N_r + N_{|r|r}|r - d_{cr}|)$, is the hydrodynamic damping matrix, where X_u, $X_{|u|u}$, Y_v, $Y_{|v|v}$, Z_w, $Z_{|w|w}$, K_p, $K_{|p|p}$, M_q, $M_{|q|q}$, N_r, and $N_{|r|r}$ are hydrodynamic damping coefficients.

R is the restoring forces and moments caused by gravity and buoyancy (Anderlini et al.,2018). Assuming buoyancy is equal to gravity, *i.e.*, $B = mg$, where g is the gravity acceleration. In addition, assume the coordinates of the floating center of the ROV in the body frame is $(x_b, y_b, z_b) = (0,0,0)$.Then:

$$R = \begin{bmatrix} (mg-B)\sin\theta \\ -(mg-B)\cos\theta\sin\varphi \\ -(mg-B)\cos\theta\cos\varphi \\ y_b B\cos\theta\cos\varphi - z_b B\cos\theta\sin\varphi \\ -z_b B\sin\theta - x_b B\cos\theta\cos\varphi \\ x_b B\cos\theta\sin\varphi + y_b B\sin\theta \end{bmatrix} = \begin{bmatrix} 0 \\ 0 \\ 0 \\ 0 \\ 0 \\ 0 \end{bmatrix} \tag{17}$$

where (x_b, y_b, z_b) is the coordinates of the floating center of the ROV in the body frame.

$\tau = [F_x, F_y, F_z, M_x, M_y, M_z]^{\mathrm{T}}$ are the propulsion forces and moments applied to the ROV. F_x, F_y and F_z are the forces along the three coordinate axes generated by the propellers. M_x, M_y and M_z are the moments around the three coordinate axes generated by the propellers.

The ocean current disturbance is explicitly considered in the constructed dynamics model, which is helpful to analyze the influence of ocean current disturbance on the ROV dynamic performance and to improve tracking accuracy. Various types of ocean current disturbance models can be adopted in the ROV dynamics model. In the subsequent experiments, we will consider the LTI disturbance and Gaussian disturbance.

3. ESKF-based MPC controller

The overall control architecture is shown in Fig.3. An ESKF-based MPC controller predicts the future state within the predictive horizon based on the current ROV state. The optimizer calculates the optimal control input that minimizes the cost function. Finally, the desired propulsion distribution block calculates the desired propulsion of each propeller.

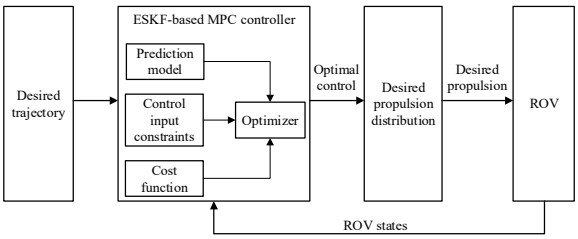

Fig.3. The overall control architecture

This paper aims at solving the three-dimensional trajectory tracking problem for ROVs in the presence of ocean current disturbance and measurement noises. Ocean current disturbance and measurement noises are added in the state prediction and output prediction processes of ESKF-based MPC, respectively. This allows ocean current disturbance and measurement noises to be considered in the control process. Based on the error between the predicted output and the desired trajectory combined with the control input increment, an objective function is constructed to ensure tracking accuracy and to prevent damages to actuators. Combined with the physical constraints of the ROV, the LTI constraints of control input are taken into account, which makes trajectory tracking more in line with actual engineering applications and is beneficial for improving tracking accuracy. In each prediction process, the optimal control input sequence in the prediction horizon can be obtained by minimizing the objective function, and the first element in the sequence is used as the control input to actuators (Nakagaki and Zhai, 2020), driving the ROV to track the pre-desired trajectory.

The ROV dynamic model in (5) can be written as:

$$\dot{V} = -M^{-1}(C+D)V + M^{-1}\tau + M^{-1}(C+D)d_c \tag{18}$$

Based on the ROV kinematics model in (1) and (18), a continuous varying nonlinear model can be obtained as follows:

$$\dot{X} = \begin{bmatrix} O_{6\times6} & G \\ O_{6\times6} & -M^{-1}(C+D) \end{bmatrix} X + \begin{bmatrix} O_{6\times6} \\ M^{-1} \end{bmatrix} \tau + \begin{bmatrix} O_{6\times6} \\ M^{-1}(C+D) \end{bmatrix} d_c \tag{19}$$

with

$$X = [S, V]^{\mathrm{T}} \tag{20}$$

MPC relies on state horizon model to predict the resulting output in the future time horizon. Although nonlinear MPC is possible, linear MPC results in much less computational effort, thus enabling a real-time implementation. The continuous varying nonlinear model is discretized with the Euler method as:

$$X(k+1) = A(k)X(k) + B(k)\tau(k) + E(k)d(k) \tag{21}$$

$$Y(k) = K(k)X(k) + F(k)n(k) \tag{22}$$

with

$$X(k) = \begin{bmatrix} S(k) \\ V(k) \end{bmatrix} \tag{23}$$

$$A(k) = \begin{bmatrix} I_{6\times6} & GT \\ O_{6\times6} & I_{6\times6} - M^{-1}(C+D)T \end{bmatrix} \tag{24}$$

$$B(k) = \begin{bmatrix} O_{6\times6} \\ M^{-1}T \end{bmatrix} \tag{25}$$

$$E(k) = \begin{bmatrix} O_{6\times6} \\ M^{-1}(C+D)T \end{bmatrix} \tag{26}$$

$$d(k) = d_c(k) \tag{27}$$

$$K(k) = [I_{6\times6} \quad O_{6\times6}] \tag{28}$$

In order to improve the robustness to the ocean current disturbance and measurement noises, the ocean current disturbance $d(k)$ is considered as an extended state based on the idea of extended state observer (ESO) (Bai et al., 2018), then the ESKF for estimating the ROV state and ocean current disturbance can be designed as:

$$\begin{bmatrix} \hat{X}(k+1) \\ \hat{d}(k+1) \end{bmatrix} = A_d(k) \begin{bmatrix} \hat{X}(k) \\ \hat{d}(k) \end{bmatrix} + B_d(k)\tau(k) + E_d(k)\widehat{W}(k) - U_k\left(Y(k) - K_d(k)\begin{bmatrix} \hat{X}(k) \\ \hat{d}(k) \end{bmatrix}\right) \tag{29}$$

$$Y(k) = K(k)\hat{X}(k) + F(k)n(k) \tag{30}$$

with

$$U_k = \tag{31}$$

$$-A_d(k)P_k{K_d}^{\mathrm{T}}(k)\left(K_d(k)P_k{K_d}^{\mathrm{T}}(k)+\frac{R_0}{1+\theta_0}\right)^{-1}$$

$$P_{k+1}=$$

$$(1+\theta_0)\big(A_d(k)+U_kK_d(k)\big)P_k\big(A_d(k)+U_kK_d(k)\big)^{\mathrm{T}} \quad (32)$$

$$+U_kR_0{U_k}^{\mathrm{T}}+\frac{1+\theta_0}{\theta_0}Q_{1,k}+Q_{2,k}$$

$$A_d(k)=\begin{bmatrix} I_{6\times6} & GT & O_{6\times6} \\ O_{6\times6} & I_{6\times6}-M^{-1}(C+D)T & M^{-1}(C+D)T \\ O_{6\times6} & O_{6\times6} & I_{6\times6}\end{bmatrix} \quad (33)$$

$$B_d(k)=\begin{bmatrix} O_{6\times6} \\ M^{-1}T \\ O_{6\times6}\end{bmatrix} \quad (34)$$

$$E_d(k)=\begin{bmatrix} O_{6\times6} \\ I_{6\times6}\end{bmatrix} \quad (35)$$

$$Q_{1,k}=\begin{bmatrix} O_{12\times12} & O_{12\times6} \\ O_{6\times12} & 4Q_k\end{bmatrix} \quad (36)$$

$$Q_k=6\mathrm{diag}(q_{k1},q_{k2},q_{k3},q_{k4},q_{k5},q_{k6}) \quad (37)$$

$$Q_{2,k}=\begin{bmatrix} 0.0009*I_{12\times12} & O_{12\times6} \\ O_{6\times12} & O_{6\times6}\end{bmatrix} \quad (38)$$

where ' ^ ' represents the estimation value, the estimation value of $\overline{W}(k)$ is defined as follows:

$$\hat{\overline{W}}(k)=\max\{\min\{\overline{W}(k),\sqrt{q_k}\},-\sqrt{q_k}\}, \quad (39)$$

with

$$\overline{W}(k)=\bar{d}(k+1)-\bar{d}(k) \quad (40)$$

where $\bar{d}(k)$ is the nominal value of $d(k)$.

According to the state estimation equation (29) and the current state, the control inputs and system states in the prediction horizon can be estimated. Denote the prediction horizon by N, then the control input $\bar{\tau}(k)$ and state $\bar{X}(k)$ in the prediction horizon can be described as:

$$\bar{\tau}(k)=[\tau(k|k),\tau(k+1|k),\cdots,\tau(k+N-1|k)]^{\mathrm{T}} \quad (41)$$

$$\bar{X}(k)=\left[\hat{X}(k+1|k),\hat{X}(k+2|k),\cdots,\hat{X}(k+N|k)\right]^{\mathrm{T}} \quad (42)$$

In general, $A(k)$, $B(k)$, and $E(k)$ remain unchanged in the prediction horizon, then $\bar{X}(k)$ can be represented as:

$$\bar{X}(k)=\bar{A}(k)\hat{X}(k|k)+\bar{B}(k)\tau(k-1)+U(k)H(k) \quad (43)$$

$$+\bar{E}(k)\hat{\bar{d}}(k)$$

where

$$\bar{A}(k)=[A(k),A(k)^2,\cdots,A(k)^N]^{\mathrm{T}} \quad (44)$$

$$\bar{B}(k)=\begin{bmatrix} B(k) \\ B(k)+A(k)B(k) \\ \vdots \\ \sum_{i=0}^{N-1}A(k)^iB(k)\end{bmatrix} \quad (45)$$

$$U(k)=\begin{bmatrix} B(k) & 0 & \cdots & 0 \\ B(k)+A(k)B(k) & B(k) & \cdots & 0 \\ \vdots & \vdots & & \vdots \\ \sum_{i=0}^{N-1}A(k)^iB(k) & \sum_{i=0}^{N-2}A(k)^iB(k) & \cdots & B(k)\end{bmatrix} \quad (46)$$

$$=\begin{bmatrix} U_{11} & U_{12} & \cdots & U_{1N} \\ U_{21} & U_{22} & \cdots & U_{2N} \\ \vdots & \vdots & \ddots & \vdots \\ U_{N1} & U_{N2} & \cdots & U_{NN}\end{bmatrix}$$

$$H(k)=[h(k|k),h(k+1|k),\cdots,h(k+N-1|k)]^{\mathrm{T}} \quad (47)$$

$$h(k+i|k)=\tau(k+i|k)-\tau(k+i-1|k) \quad (48)$$

$$\bar{E}(k)=\begin{bmatrix} E(k) & 0 & \cdots & 0 \\ A(k)E(k) & E(k) & \cdots & 0 \\ \vdots & \vdots & \ddots & \vdots \\ A(k)^{N-1}E(k) & A(k)^{N-2}E(k) & \cdots & E(k)\end{bmatrix} \quad (49)$$

$$\hat{\bar{d}}(k)=\mathrm{repmat}(\hat{d}(k),N,1) \quad (50)$$

where repmat is a function, which is used to construct a block matrix of N rows and one column with $\hat{d}(k)$.

When designing the trajectory tracking controller based on MPC, it is necessary to consider the LTI constraints of control input increment. Control input increment $h(k)$ has its explicit lower bound and upper bound as follows:

$$h_{min}\le h(k)\le h_{max} \quad (51)$$

where h_{min} is a predefined lower bound, h_{max} is a predefined upper bound.

Then the following constraints can be obtained:

$$H(k)\le H_{max} \quad (52)$$

$$-H(k)\le -H_{min} \quad (53)$$

The above constraints can be expressed in the following vector form:

$$LH(k)\le l \quad (54)$$

where

$$L=[I_{6N\times6N},-I_{6N\times6N}]^{\mathrm{T}} \quad (55)$$

$$l=[H_{max},-H_{min}]^{\mathrm{T}} \quad (56)$$

$$H_{max}=\mathrm{repmat}(h_{max},N,1) \quad (57)$$

$$H_{min} = \text{repmat}(h_{min}, N, 1) \tag{58}$$

The cost function is constructed based on the error between the predicted trajectory and the expected trajectory combined with the control input increment (Gan et al.,2019). The cost function is defined as follows:

$$J(k) = \sum_{i=1}^{N} (\|Y(k+i|k) - Y_d(k+i)\|_{Q_y}^2 + \|h(k+i-1|k)\|_{Q_u}^2) \tag{59}$$

The first term is the tracking error penalty, which is used to ensure the tracking accuracy. $Y(k+i|k)$ is the predicted position at time $k+i$, $Y_d(k+i)$ is the desired position at time $k+i$, $Y(k+i|k) - Y_d(k+i)$ is the tracking error at time $k+i$, Q_y is the state weight matrix. The second term is the control input penalty, which helps to avoid speed jerk and to make trajectory tracking more robust. $h(k+i-1|k)$ is the control input increment at time $k+i$, and Q_u represents the control input weight matrix.

Since $Y(k) = K(k)\hat{X}(k) + F(k)n(k)$, the cost function can be further transformed into the following form:

$$J(k) = \|\bar{X}(k) - \overline{X_d}(k)\|_{\bar{Q}_x}^2 + \|H(k)\|_{\bar{Q}_u}^2 + \sum_{i=1}^{N} \hat{X}^{\mathrm{T}}(k+i|k)K^{\mathrm{T}}(k)Q_yF(k)n(k) + \sum_{i=1}^{N} n^{\mathrm{T}}(k)F^{\mathrm{T}}(k)Q_yK(k)\hat{X}(k+i|k) \tag{60}$$

where

$$\bar{Q}_x = \text{blkdiag}(Q_x, Q_x, Q_x, Q_x, Q_x, Q_x, Q_x, Q_x, Q_x, Q_x) \tag{61}$$

$$\bar{Q}_u = \text{blkdiag}(Q_u, Q_u, Q_u, Q_u, Q_u, Q_u, Q_u, Q_u, Q_u, Q_u) \tag{62}$$

$$Q_x = K^{\mathrm{T}}(k)Q_yK(k) \tag{63}$$

where blkdiag is a function, which is used to construct a block diagonal matrix with Q_x.

Then:

$$\begin{aligned}&\|\bar{X}(k) - \overline{X_d}(k)\|_{\bar{Q}_x}^2 = \\ &H^{\mathrm{T}}(k)U^{\mathrm{T}}(k)\bar{Q}_x(\bar{A}(k)\hat{X}(k|k) \\ &+\bar{B}(k)\tau(k-1) + \bar{E}(k)\hat{\bar{d}}(k) - \overline{X_d}(k)) \\ &+(\hat{X}^{\mathrm{T}}(k|k)\bar{A}^{\mathrm{T}}(k) + \tau^{\mathrm{T}}(k-1)\bar{B}^{\mathrm{T}}(k) + \hat{\bar{d}}^{\mathrm{T}}(k)\bar{E}^{\mathrm{T}}(k) \\ &-\overline{X_d}^{\mathrm{T}}(k))\bar{Q}_xU(k)H(k) + H^{\mathrm{T}}(k)U^{\mathrm{T}}(k)\bar{Q}_xU(k)H(k) \\ &+constant\end{aligned} \tag{64}$$

$$\sum_{i=1}^{N} \hat{X}^{\mathrm{T}}(k+i|k)K^{\mathrm{T}}(k)Q_yF(k)n(k) = \tag{65}$$

$$\begin{aligned}&H^{\mathrm{T}}(k)\left[\sum_{i=1}^{N} U_{i1}, \sum_{i=1}^{N} U_{i2}, \cdots, \sum_{i=1}^{N} U_{iN}\right]^{\mathrm{T}} \\ &\times K^{\mathrm{T}}(k)Q_yF(k)n(k) + constant \\ &\sum_{i=1}^{N} n^{\mathrm{T}}(k)F^{\mathrm{T}}(k)Q_yK(k)\hat{X}(k+i|k) = \\ &P(k)\left[\sum_{i=1}^{N} U_{i1}, \sum_{i=1}^{N} U_{i2}, \cdots, \sum_{i=1}^{N} U_{iN}\right]H(k) + constant\end{aligned} \tag{66}$$

where

$$P(k) = n^{\mathrm{T}}(k)F^{\mathrm{T}}(k)Q_yK(k) \tag{67}$$

Ignore the constant term, then the cost function can be further written as:

$$\begin{aligned}&J(k) = ((\hat{X}^{\mathrm{T}}(k|k)\bar{A}^{\mathrm{T}}(k) + \tau^{\mathrm{T}}(k-1)\bar{B}^{\mathrm{T}}(k) \\ &+\hat{\bar{d}}^{\mathrm{T}}(k)\bar{E}^{\mathrm{T}}(k) - \overline{X_d}^{\mathrm{T}}(k))\bar{Q}_xU(k) \\ &+P(k)\left[\sum_{i=1}^{N} U_{i1}, \sum_{i=1}^{N} U_{i2}, \cdots, \sum_{i=1}^{N} U_{iN}\right])H(k) \\ &+H^{\mathrm{T}}(k)(U^{\mathrm{T}}(k)\bar{Q}_xU(k) + \bar{Q}_u)H(k) \\ &+H^{\mathrm{T}}(k)(U^{\mathrm{T}}(k)\bar{Q}_x(\bar{A}(k)X(k|k) \\ &+\bar{B}(k)\tau(k-1) + \bar{E}(k)\hat{\bar{d}}(k) - \overline{X_d}(k)) \\ &+\left[\sum_{i=1}^{N} U_{i1}, \sum_{i=1}^{N} U_{i2}, \cdots, \sum_{i=1}^{N} U_{iN}\right]^{\mathrm{T}} \\ &\times K^{\mathrm{T}}(k)Q_yF(k)n(k))\end{aligned} \tag{68}$$

That is:

$$J(k) = \frac{1}{2}H^{\mathrm{T}}(k)\alpha(k)H(k) + \beta^{\mathrm{T}}(k)H(k) + H^{\mathrm{T}}(k)\gamma(k) \tag{69}$$

where

$$\alpha(k) = 2(U^{\mathrm{T}}(k)\bar{Q}_xU(k) + \bar{Q}_u) \tag{70}$$

$$\begin{aligned}&\beta(k) = \\ &((\hat{X}^{\mathrm{T}}(k|k)\bar{A}^{\mathrm{T}}(k) + \tau^{\mathrm{T}}(k-1)\bar{B}^{\mathrm{T}}(k) \\ &+\hat{\bar{d}}^{\mathrm{T}}(k)\bar{E}^{\mathrm{T}}(k) - \overline{X_d}^{\mathrm{T}}(k))\bar{Q}_xU(k) + \\ &P(k)\left[\sum_{i=1}^{N} U_{i1}, \sum_{i=1}^{N} U_{i2}, \cdots, \sum_{i=1}^{N} U_{iN}\right])^{\mathrm{T}}\end{aligned} \tag{71}$$

$$\begin{aligned}&\gamma(k) = U^{\mathrm{T}}(k)\bar{Q}_x(\bar{A}(k)\hat{X}(k|k) \\ &+\bar{B}(k)\tau(k-1) + \bar{E}(k)\hat{\bar{d}}(k) - \overline{X_d}(k)) \\ &+\left[\sum_{i=1}^{N} U_{i1}, \sum_{i=1}^{N} U_{i2}, \cdots, \sum_{i=1}^{N} U_{iN}\right]^{\mathrm{T}} \\ &\times K^{\mathrm{T}}(k)Q_yF(k)n(k)\end{aligned} \tag{72}$$

In order to compute the optimal control input increment sequence $H^*(k)$ in the current state, we construct the objective function based on the above cost function as follows:

$$H^*(k) = {}^{argmin}_{H(k)} J(k)$$
$$s.t.\ LH(k) \le l \tag{73}$$

Solving the above objective function under the provided constraints can yield the optimal control input increment sequence $H^*(k)$ in the current state. Denote the first element of $H^*(k)$ as $H_1^*(k)$. Then, the expected propulsions and moments of the propellers can be obtained as follows:

$$\tau(k) = \tau(k-1) + H_1^*(k) \tag{74}$$

After obtaining the propulsions and moments, the expected propulsion vector F_p for each propeller can be calculated:

$$F_p = {T_r}^{-1}\tau \tag{75}$$

where

$$T_r = [T_{r1} \quad T_{r2}] \tag{76}$$

$$T_{r1} = \begin{bmatrix} cos\delta & cos\delta & -cos\delta & -cos\delta \\ sin\delta & -sin\delta & sin\delta & -sin\delta \\ 0 & 0 & 0 & 0 \\ z_h sin\delta & -z_h sin\delta & z_h sin\delta & -z_h sin\delta \\ -z_h cos\delta & -z_h cos\delta & z_h cos\delta & z_h cos\delta \\ -y_h cos\delta - x_h sin\delta & y_h cos\delta + x_h sin\delta & y_h cos\delta + x_h sin\delta & -y_h cos\delta - x_h sin\delta \end{bmatrix} \tag{77}$$

$$T_{r2} = \begin{bmatrix} sin\sigma & sin\sigma & -sin\sigma \\ 0 & 0 & 0 \\ cos\sigma & cos\sigma & cos\sigma \\ y_v cos\delta & -y_v cos\delta & 0 \\ z_v sin\delta + x_v cos\delta & z_v sin\delta + x_v cos\delta & -z_v sin\delta - x_v cos\delta \\ -y_v \sin\delta & -y_v \sin\delta & 0 \end{bmatrix} \tag{78}$$

where ${T_r}^{-1}$ is the inverse of T_r. δ is the angle between the axis of each horizontal propeller and axis X_b, σ is the angle between the axis of each vertical propeller and the axis Z_b. x_h, y_h, and z_h are the distances between the axis of each horizontal propeller and X_b, Y_b, and Z_b, respectively. x_v, y_v and z_v are the distances between the axis of each vertical propeller and X_b, Y_b, and Z_b, respectively.

In this section, we have derived the discrete-time varying nonlinear model of ESKF-based MPC based on the kinematics model and dynamics model of the ROV, and have introduced measurement noise into the output equation, which is conducive to improving the robustness to measurement noise. In addition, we have considered LTI constraints on control input increment, which helps make control closer to actual use. In order to ensure tracking accuracy and prevent damages to actuators, we have also constructed an objective function based on the tracking error and the control input increment. Based on the optimal control input increment calculated by the objective function, we have finally obtained the desired propulsion needed to drive the ROV.

4. Simulations

In this section, simulations of a tracking three-dimensional sine curve and a spiral curve are carried out, which are usually used by researchers to verify the trajectory tracking performance of the ROV.

The key ROV parameters are shown in the Table 1. The simulation setups are as follows: initial speed $V_0 = [0,0,0,0,0,0]^{\mathrm{T}}$, the unit of the first three values in this vector is $\mathrm{m/s}$, and the unit of the last three values is $\mathrm{rad/s}$, prediction horizon $N = 10$, sampling period $T = 0.5s$, the weighting matrices $Q_y = \mathrm{diag}(1,1,1,1,1,1)$, $Q_u = \mathrm{diag}(1,1,1,1,1,1)$, constraints on control input $h_{max} = [300,300,300,150,150,150]^{\mathrm{T}}$, the unit of the first three values in this vector is N, and the unit of the last three values is $\mathrm{N \cdot m}$, $h_{min} = [-300,-300,-300,-150,-150,-150]^{\mathrm{T}}$, the unit of the first three values in this vector is N, and the unit of the last three values is $\mathrm{N \cdot m}$, $F(k) = \mathrm{diag}(0.4,0.3,0.2,0.4,0.3,0.2)$, $n(k) = [\ \mathrm{randn}(1)\ ,\ \mathrm{randn}(1)\ ,\ \mathrm{randn}(1),\ \mathrm{randn}(1),\ \mathrm{randn}(1),\ \mathrm{randn}(1)]^{\mathrm{T}}$, the unit of the first three values in this vector is m, and the unit of the last three values is rad, $R_0 = 0.0009 * I_{6\times6}$, $\theta_0 = 0.000001$, $q_k = 0.001 * [1,1,1,1,1,1]$, $q_{k,i} = 0.001, i = 1,2,3,4,5,6$.

Each simulation experiment will be carried out under three conditions: no ocean current disturbance, constant ocean current disturbance, and random ocean current disturbance. Denote by dc_i the ocean current disturbance vector relative to the inertial reference frame. We consider constant ocean current disturbance vector $dc_i = [-0.3,0.3,0.3,0,0,0]^{\mathrm{T}}$, and random ocean current disturbance vector $dc_i = [0.3\mathrm{randn}(1),\ 0.3\mathrm{randn}(1),\ 0.3\mathrm{randn}(1),\ 0,\ 0,\ 0]^{\mathrm{T}}$, with unit being m/s.

4.1. Tracking of a three-dimensional sine curve

The first curve tracked by the ROV is a three-dimensional sine curve. The expression of the sine curve is as follows:

$$\begin{cases} x_d = t \\ y_d = 25sin(0.1t) \\ z_d = 3t/10 - 50 \end{cases} \quad 0 \le t < 100 \tag{79}$$

The initial ROV position and attitude of the three-dimensional sine curve tracking simulation is $S_{sin} = [5,5,-45,0,0,0]^{\mathrm{T}}$, the unit of the first three values in this vector is m, and the unit of the last three values is rad.

Results are shown in Fig.4 and Fig.5. Position errors after the ROV has moved for 5 minutes are shown in Fig.6 and Fig.7. From Fig.6 and Fig.7, it can be seen that tracking errors when there are no measurement noises are smaller than those with measurement noises. It can be known from the calculation that average tracking errors under three different conditions without measurement noises are 0.0031m, 0.0032m, and 0.0033m, respectively. Average tracking errors under three different conditions with measurement noises are 0.0871m, 0.1009m, 0.1014m, respectively. it is shown that the tracking error under random ocean current disturbance is the largest, followed by the tracking error under constant ocean current disturbance, then the tracking error without ocean current disturbance. This is because the ocean current disturbance causes the ROV to deviate from the desired trajectory. The tracking errors rapidly decrease to a small value approaching to 0 in about 5 seconds and the errors in the whole tracking process are very small. In addition, root mean square errors under three different conditions without measurement noises are 0.0019m, 0.0021m, and 0.0018m, respectively. Root mean square errors under three different conditions with measurement noises are 0.0550m, 0.0657m, and 0.0588m, respectively. By comparing these values, it is found that tracking errors when there are measurement noises are more fluctuating than those with no measurement noises. This is because sensor noises can interfere with position measurement. All in all, tracking errors rapidly decrease to a small value approaching to 0 in about 5 seconds, errors and fluctuations in the whole tracking process are very small. These results demonstrate that the trajectory tracking algorithm is effective and robust.

Table 1
Parameters related to the ROV

Parameters	Value	Unit	Parameters	Value	Unit
m	4187.5	kg	Z_w	4451	kg/s
I_x	2038	kgm^2	K_p	5013	$kgm^2/(s \cdot rad)$
I_y	3587	kgm^2	M_q	4527	$kgm^2/(s \cdot rad)$
I_z	3587	kgm^2	N_r	5684	$kgm^2/(s \cdot rad)$
$X_{\dot{u}}$	-3179	kg	$X_{\|u\|u}$	1924	kg/m
$Y_{\dot{v}}$	-4546	kg	$Y_{\|v\|v}$	2381	kg/m
$Z_{\dot{w}}$	-7282	kg	$Z_{\|w\|w}$	517	kg/m
$K_{\dot{p}}$	-4516	kgm^2	$K_{\|p\|p}$	1513	kgm^2/rad^2
$M_{\dot{q}}$	-6035	kgm^2	$M_{\|q\|q}$	2178	kgm^2/rad^2
$N_{\dot{r}}$	-3614	kgm^2	$N_{\|r\|r}$	2033	kgm^2/rad^2
X_u	1347	kg/s	g	9.8	m/s^2
Y_v	2401	kg/s	x_b	0	m
y_b	0	kg	z_b	-0.39	m
δ	$\pi/4$	rad	σ	$\pi/12$	rad

x_h	1.155	m	y_h	0.555	m
z_h	0.6	m	x_v	1	m
y_v	0.555	m	z_v	0.6	m

Desired propulsions required for 7 propellers are plotted in Fig.8. It can be seen from Fig.8 that expected propulsions of these propellers calculated according to the obtained optimal control input are smooth, which is conducive to the control of propellers.

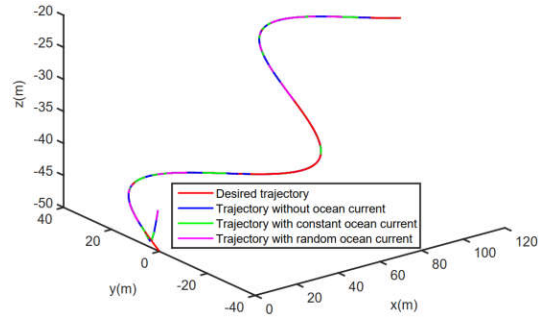

Fig.4. ROV trajectories for the 3D sine curve under different disturbances without measurement noises

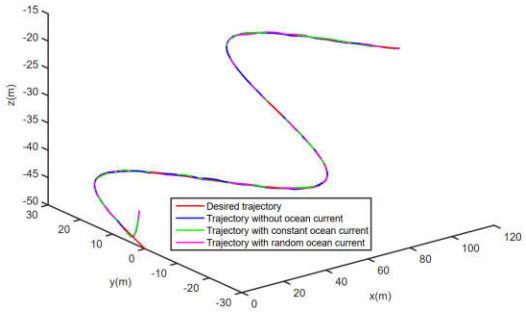

Fig.5. ROV trajectories for the 3D sine curve under different disturbances with measurement noises

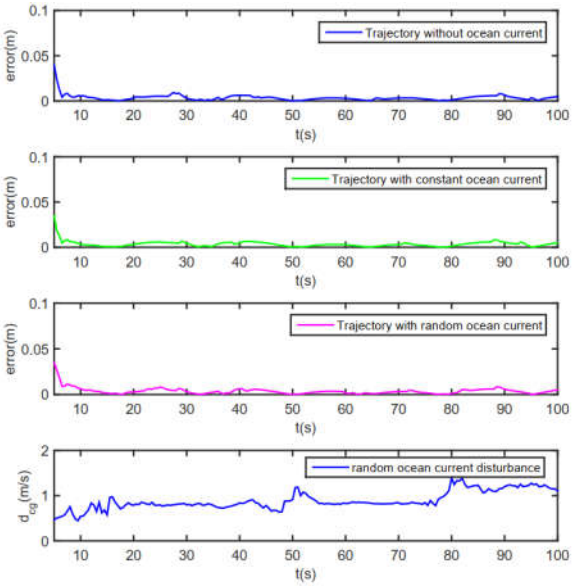

Fig.6. Position tracking errors for tracking the 3D sine curve under different disturbances without measurement noises

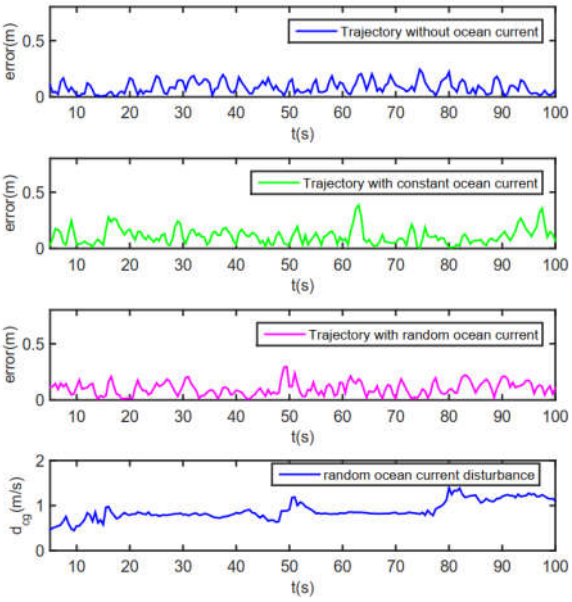

Fig.7. Position tracking errors for tracking the 3D sine curve under different disturbances with measurement noises

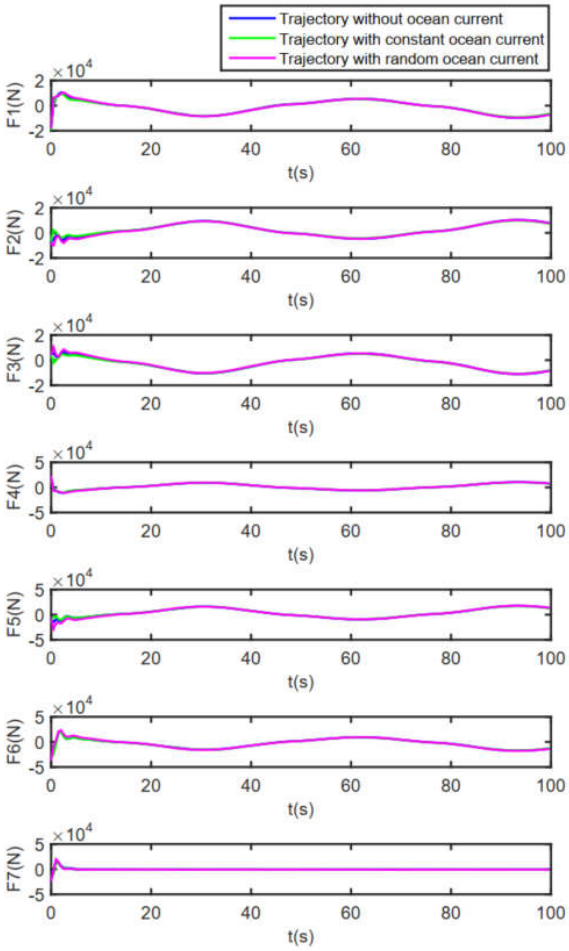

Fig.8. Propulsions of propellers for tracking the 3D sine curve under different disturbances

4.2. Tracking of a three-dimensional spiral curve

The second curve tracked by the ROV is a three-dimensional spiral curve. The expression of the spiral curve is as follows:

$$\begin{cases} x_d = 10sin(0.03t) \\ y_d = 10cos(0.03t) \\ z_d = -0.05t \end{cases} \quad 0 \le t < 200 \tag{80}$$

The initial ROV position and attitude in the three-dimensional spiral curve tracking simulation is $S_{spi} = [0,5,0,0,0,0]^{\mathrm{T}}$, the unit of the first three values in this vector is m, and the unit of the last three values is rad.

Results are shown in Fig.9 and Fig.10. Errors of

tracking the three-dimensional spiral curve after the ROV has moved for 5 minutes are shown in Fig.11 and Fig.12. Average errors and root mean square errors of tracking under three different conditions with or without measurement noises are listed in Table 2.

Table 2
Average errors and root mean square (RMS) errors under three different conditions with or without measurement noises

Disturba-nces	Noises	Average(m)	RMS(m)
without	without	0.00030	0.00035
	with	0.1001	0.0731
constant ocean current	without	0.00032	0.00029
	with	0.1076	0.0730
random ocean current	without	0.00035	0.00034
	with	0.1143	0.0654

From Fig.11, Fig.12 and Table 2, similar observations can be made as tracking the three-dimensional sine curve. In addition, errors and fluctuations in the whole tracking process are also very small. Tracking results show that the trajectory tracking algorithm can converge and stabilize quickly.

Desired propulsions required for 7 propellers under measurement noises are plotted in Fig.13. At the beginning of simulations, desired propulsions change quickly since the initial position of ROV is not the same as the starting point of the desired trajectory. However, the expected propulsions remain basically unchanged after stabilization, while desired propulsions when tracking the spiral curve change sinusoidally with time. In the meantime, there is no problem of chattering, which helps to avoid damage to propellers.

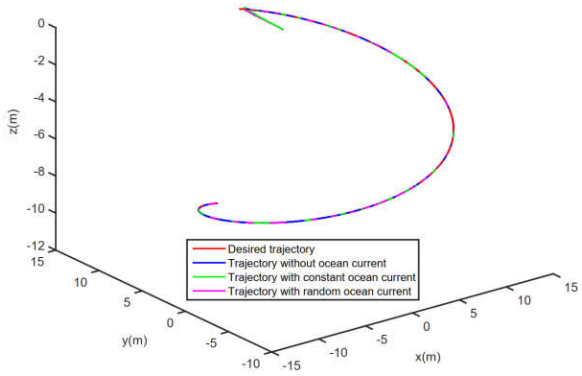

Fig.9. ROV trajectories during tracking the 3D spiral curve under different disturbances without measurement noises

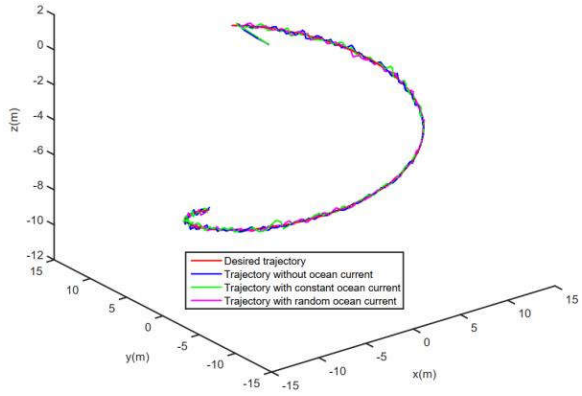

Fig.10. ROV trajectories during tracking the 3D spiral curve under different disturbances with measurement noises

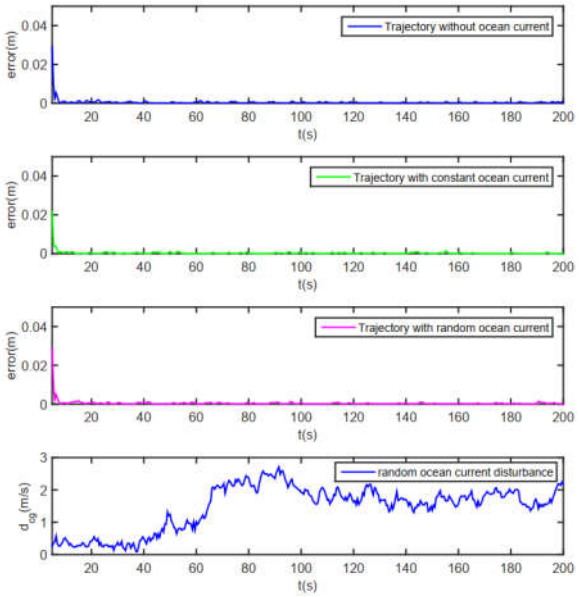

Fig.11. Position tracking errors for tracking the 3D spiral curve under different disturbances without measurement noises

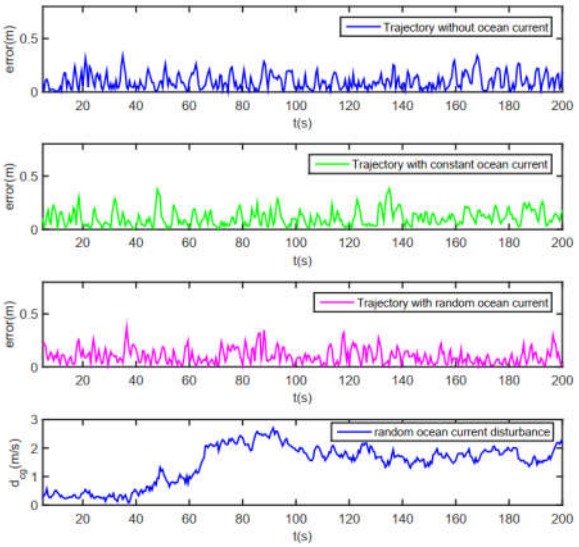

Fig.12. Position tracking errors for tracking the 3D spiral curve under different disturbances with measurement noises

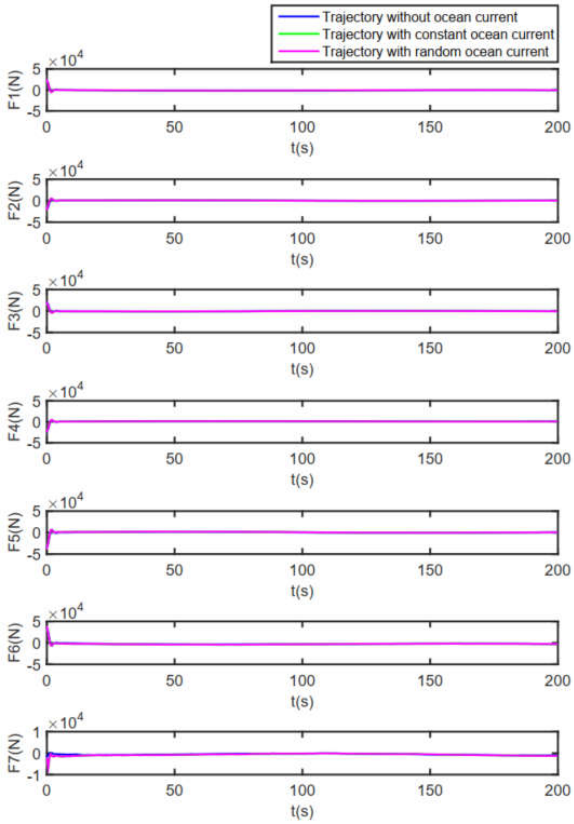

Fig.13. Propulsions of propellers for tracking the 3D spiral curve under different disturbances

5. Conclusion

In this paper, a method for trajectory tracking of a six-degree-of-freedom ROV is designed based on ESKF-based MPC. First, the kinematics model and the dynamics model of the ROV are established, where the assumption that the centre of gravity of the ROV coincides with the centre of buoyancy is made. The ocean current disturbance is introduced into the dynamics model in the form of velocities rather than forces, which helps avoid the issue of unmeasurable forces caused by the ocean current. Second, a discrete-time varying nonlinear model is constructed based on the proposed ROV kinematics and dynamics, where the Euler method is used. Process disturbance caused by the ocean current disturbance is considered in the process of state prediction and measurement noises are

considered in the process of output prediction. Third, ESKF is constructed to estimate system states and the ocean current disturbance in the presence of measurement noises in order to improve the resistance of the tracking algorithm to the ocean current disturbance and measurement noises. Fourth, LTI constraints of the control input increment are taken into account. Fifth, the ESKF-based MPC controller in the presence of the ocean current disturbance and measurement noises is newly formulated and an objective function is established based on the tracking error and the control input increment to transform the trajectory tracking problem into an optimization problem under LTI constraints, which is beneficial for ensuring tracking accuracy and preventing damage to actuators. Finally, simulation results of tracking two different types of curves show the effectiveness and robustness of the controller in the presence of the ocean current disturbance and measurement noises.

In the future research, model uncertainties and experiments in real seas will be considered.

Acknowledgments

This study was supported by Key R&D Program of Hunan Province with 2019GK2161, the Major S&T Program of Hunan Province with 2020GK1020, and State Key Laboratory of Advanced Design and Manufacturing for Vehicle Body with 61775006.

References

[1] Anderlini,E., Parker, G.G. , &Thomas,G.,2018. Control of a rov carrying an object. Ocean Engineering, 165(OCT.1), 307-318.

[2] Bai,G., Meng,Y., Liu,L., Luo,W., &Gu, Q.,2019. Review and comparison of path tracking based on model predictive control. Electronics, 8(10), 1077-.

[3] Bai,W., Xue,W., Huang,Y., & Fang,H.,2018. On extended state based kalman filter design for a class of nonlinear time-varying uncertain systems. *Science China Information Sciences*, *61*(04),1-16.

[4] Boehm,J., Berkenpas,E., Shepard,C., &Paley,D.A.,2020. Tracking performance of model-based thruster control of a remotely operated underwater vehicle.IEEE Journal of Oceanic Engineering,PP(99),1-13.

[5] Choyekh,M., Kato,N., Short,T., Ukita,M., Yamaguchi,Y., &Senga,H.,et al,201).Vertical water column survey in the gulf of mexico using autonomous underwater vehicle sotab-i. Marine Technology Society Journal,49(3),88-101.

[6] Chu,Z., Zhu,D., &Jan,G.E.,2016.Observer-based adaptive neural network control for a class of remotely operated vehicles.Ocean Engineering, 127(nov.15),82-89.

[7] Cui,R., Yang,C., Li,Y., &Sharma, S.,2017. Adaptive neural network control of auvs with control input nonlinearities using reinforcement learning. IEEE Transactions on Systems Man & Cybernetics Systems, 47(6),1019-1029.

[8] Dai,J., Zhao,X., &Min,T.,2002. Fuzzy logic control in autonomous ROV navigation.

[9] Fossen T.I, Ross A,2006. Guidance and Control of unmanned marine vehicles,IEEE Contr. Eng.Series(Peregrinus,Stevengce),23-42.

[10] Gan, W., Zhu, D., Hu, Z., Shi, X., & Chen, Y.,2019.Model predictive adaptive constraint tracking control for underwater vehicles. IEEE Transactions on Industrial Electronics, PP(99), 1-1.

[11] Khodayari,M.H., & Balochian,S,2015. Modeling and control of autonomous underwater vehicle (auv) in heading and depth attitude via self-adaptive fuzzy pid controller. Journal of Marine Science and Technology, 20(3), 559-578.

[12] Kim,M., Joe,H., Pyo,J., Kim,J., Kim,H., &Yu,S.C,2013. Variable-structure PID controller with anti-windup for autonomous underwater vehicle.In 2013 OCEANS-San Diego (pp.1-5).IEEE.

[13] Liu,S., Wei,Y., &Gao,Y.,2012. 3D path planning for AUV using fuzzy logic. Computer Science and Information Processing (CSIP), 2012 International Conference on. IEEE.

[14] Molero,A., Dunia,R., Cappelletto,J., &Fernandez,G.,2012. Model predictive control of remotely operated underwater vehicles. IEEE Conference on Decision & Control & European Control Conference.IEEE.

[15] Mon,Y. J., &Lin,C.M.,2012. Supervisory recurrent fuzzy neural network guidance law design for autonomous underwater vehicle. International Journal of Fuzzy Systems, 14(1),54-64.

[16] Nakagaki,Y., &Zhai,G.,2020. A study on optimization algorithms in mpc. Journal of Physics Conference Series, 1490, 012073.

[17] Qiao,L., & Zhang,W.,2018. Adaptive second-order fast nonsingular terminal sliding mode tracking control for fully actuated autonomous underwater vehicles.IEEE Journal of Oceanic Engineering,44(2),363-385.

[18] Repoulias,F., &Papadopoulos,E.,2006. Trajectory Planning and Tracking Control of Underactuated AUVs. IEEE International Conference on Robotics & Automation.IEEE.

[19] Roche,E., Sename,O., &Simon,D.,2009. Lpv/H_∞ control of an autonomous underwater vehicle(auv.Transactions of the Chinese Society for Agricultural Machinery, 42(10), 6-12.

[20] Shen,C., Buckham,B., &Shi,Y.,2017. Modified c/gmres algorithm for fast nonlinear model predictive tracking control of auvs. IEEE Transactions on Control Systems Technology, 25(5), 1896-1904.

[21] Shen,C., Shi,Y., &Buckham,B.,2017(a). Trajectory tracking control of an autonomous underwater vehicle using lyapunov-based model predictive control.IEEE Transactions on Industrial Electronics, PP(99),1-1.

[22] Shen,C., Shi,Y., &Buckham,B.,2017(b). Integrated path planning and tracking control of an auv: a unified receding horizon optimization approach. IEEE/ASME Transactions on Mechatronics,22(99),1163-1173.

[23] Soylu,S., Proctor,A.A., Podhorodeski,R.P., Bradley,C., &Buckham, B.J.,2016. Precise trajectory control for an inspection class rov. Ocean Engineering, 111(JAN.1),508-523.

[24] Sun,B., Zhu,D., &Yang,S.X.,2018. An optimized fuzzy control algorithm for three-dimensional auv path planning. International Journal of Fuzzy Systems,20(2),597-610.

[25] Tsukioka,S., Aoki,T., Yamamoto,I., Yoshida,H., Hyakudome,T., &Sawa, T.,et al,2005.The pem fuel cell system for autonomous underwater vehicles.Marine Technology Society Journal,39(3),56-64.

[26] Wang, L., Jia,H.M., Zhang,L.J., Yang,L.X., &Wang,H.B.,2011. Iterative Sliding Mode Control for Path-Following of Underactuated AUV.
[27] Yan,Z., Gong,P., Zhang,W., &Wu,W.,2020. Model predictive control of autonomous underwater vehicles for trajectory tracking with external disturbances. Ocean Engineering,217,107884.
[28] Zain,Z.M., Pebrianti,D., &Harun,N.,2014. Stabilization control for an x4-auv using backstepping control method. Australian Journal of Basic &Applied Sciences.
[29] Zhang,Y., Liu,X., Luo,M., &Yang,C.,2019. Mpc-based 3D trajectory tracking for an autonomous underwater vehicle with constraints in complex ocean environments. Ocean Engineering,189, 106309.
[30] Zhou,B., Satyavada,H., &Baldi,S.,2017. Adaptive path following for Unmanned Aerial Vehicles in time-varying unknown wind environments. American Control Conference.IEEE.
[31] Zhu,B., &Xia,X.,2016. Adaptive model predictive control for unconstrained discrete-time linear systems with parametric uncertainty. IEEE Transactions on Automatic Control, 61(10), 3171-3176.